Asociación Argentina
de Mecánica Computacional

Mecánica Computacional Vol XXIX, págs. 3485-3497 (artículo completo)
Eduardo Dvorkin, Marcela Goldschmit, Mario Storti (Eds.)
Buenos Aires, Argentina, 15-18 Noviembre 2010

EXTENDED FINITE ELEMENT METHOD FOR FLUID-STRUCTURE INTERACTION PROBLEMS

H.C. Gomes and P.M. Pimenta

Polytechnic School at University of São Paulo, Brazil, [henrique.campelo,ppimenta]@usp.br

Keywords: Fluid-structure interaction, Extended Finite Element Method, Incompressible fluid flow.

Abstract. This work proposes a study on the XFEM method used to treat the conjoined interface between fluid and structure domains in two dimensional coupled Fluid-Structure Interaction (FSI) problems. The idea is based on [1], in which the FSI problem is solved adopting two non-matching overlapping meshes for the structural and fluid fields in an alternative to usual Arbitrary Lagrangian Eulerian (ALE) approaches. Using this formulation, the fluid can be solved by classical Eulerian approach where the mesh is fixed in space during all the computation. In order to illustrate the method applicability, steady and unsteady simulations of incompressible viscous flow past a cylinder were performed.

1 INTRODUCTION

Fluid-structure interaction problems are of great importance for many engineering fields and thus the development of robust computational codes is desired by many research groups throughout the world. Most of the approaches to solve the problems, commercial or academic, lacks robustness or efficiency in some situations. Such situations are, for example, simulations in which the fluid and the structure have similar densities, like blood and tissues in problems of biomechanics [5]. Another situation difficult to overcome by standard approaches is that in which the structure surface exhibits large and complex motion. In this kind of problem, the fluid flow at the neighborhoods of the structure is strongly affected by its motion and most codes fail in simulating this behavior accurately. Methods based on ALE approach formulate and solve the fluid field on a deforming grid. This grid deforms with the structure at the interface and then the grid deformation is extended into some portion of the fluid field. As the fluid grid is attached to the structure interface, it is not possible to preserve the mesh under complex motion of the structure and thus this kind of problems cannot be solved by ALE approaches.

Many different methods have been proposed as an alternative to classical ALE approaches. Some of them treat both the fluid and solid domains through a Lagrangian description as in [2] and [3]. Using a Lagrangian description for the fluid domain has the advantage of eliminating the non linear convective term from the Navier-Stokes equation but, by the other hand, one needs to pay the price of remeshing the fluid grid at each time step.

This work proposed by the authors follows the trend that treat the FSI problem by two overlapping domains. The first domain, occupied by the fluid, is modeled by an unchanging fixed mesh that solves the Navier-Stokes equations for incompressible fluid flow in the traditional Eulerian approach. The second domain, in turn, occupied by the structure, is modeled using a Lagrangian description as usual. As the fluid and structure meshes are constructed in an independent manner, some special technique is required in order to impose the effects of the moving structure interface, which acts as essential boundary conditions for the fluid problem. The special technique to be adopted in this work will be the Extended Finite Element Method (XFEM) [1] with Lagrange multipliers to couple the interface conditions from both structural and fluid domains.

This work is organized in what follows: section 2 presents the main issues regarding the fluid description. Section 3 explains the imposition of the interface condition between the fluid and the structure by XFEM and, in the sequence, the discrete system of algebraic equations obtained from the finite element method is derived in section 3.2. In section 4, the algorithm used to solve the fsi coupled problem is presented. To validate the formulation exposed, in section 5, we present some examples performed and, finally, the conclusions and new developments under conduction are addressed in section 6.

2 FLUID DESCRIPTION

In this section we describe the mathematical model adopted in our formulation, that is, the Navier-Stokes equations for incompressible fluid flow. The time integration scheme and stabilization techniques used in our computational code are also considered in this section. More details on this subject can be found in a previous work by the authors [4].

2.1 Navier-Stokes Equations

The conservation of linear momentum of a fluid portion can be stated as

$$\rho \frac{\mathrm{D}\boldsymbol{u}}{\mathrm{D}t} - \mathrm{div}\,\boldsymbol{T} = \rho \boldsymbol{b}\,, \tag{1}$$

where ρ is the fluid density and b the volumetric force per unit mass. $\mathrm{D}u/\mathrm{D}t$ is the material (or substantive) time derivative of the velocity and $\boldsymbol{T}$ the Cauchy stress tensor. The mass conservation equation for incompressible fluid is

$$\mathrm{div}\boldsymbol{u} = 0\,. \tag{2}$$

Adopting an Eulerian system of reference, the material time derivative will result in two terms: the local time derivative and the convective acceleration. Equation (1) is thus rewritten as

$$\rho\left(\dot{\boldsymbol{u}} + \left(\nabla \boldsymbol{u}\right)\boldsymbol{u}\right) - \mathrm{div}\,\boldsymbol{T} = \rho \boldsymbol{b}\,, \tag{3}$$

where the dot over the velocity means a partial time derivative with respect to time. The Cauchy stress tensor, using the Newtonian material law, is given by

$$\boldsymbol{T} = -p\boldsymbol{I} + 2\mu\boldsymbol{\varepsilon}\left(\boldsymbol{u}\right). \tag{4}$$

In the previous equation, μ is the fluid dynamic viscosity, p is the pressure and $\boldsymbol{\varepsilon}$ is the strain rate tensor given by

$$\boldsymbol{\varepsilon}\left(\boldsymbol{u}\right) = \frac{1}{2}\left(\nabla \boldsymbol{u} + \left(\nabla \boldsymbol{u}\right)^{\mathrm{T}}\right). \tag{5}$$

When deriving the stress tensor in order to obtain its divergent in Eq. (1), we have

$$\mathrm{div}\boldsymbol{T} = -\nabla p + \mu\nabla^2\boldsymbol{u} + \mu\nabla\left(\mathrm{div}\boldsymbol{u}\right), \tag{6}$$

in which the last term vanishes due to the divergence free condition of incompressible fluid flow. Substituting the last equation into Eq. (3) we finally obtain

$$\begin{aligned} &\dot{\boldsymbol{u}} + \left(\nabla \boldsymbol{u}\right)\boldsymbol{u} - \nu\nabla^2\boldsymbol{u} + \nabla p = \boldsymbol{b} \\ &\mathrm{div}\boldsymbol{u} = 0\,, \end{aligned} \tag{7}$$

where the incompressibility condition was repeated here to clarify the exposition. Equations (7) are known as the Navier-Stokes equations for incompressible fluids. Note that all terms were divided by ρ in the first equation originating the fluid kinematic viscosity defined by $\nu = \mu/\rho$ and the kinematic pressure p.

The Navier-Stokes problem needs suitable initial and boundary conditions in order to become a well-posed initial boundary value problem. For that purpose, we define

$$\begin{aligned} \boldsymbol{u} &= \overline{\boldsymbol{u}} \quad \text{on} \quad \Gamma_{\boldsymbol{u}} \\ -p\boldsymbol{n} + \nu\big(\nabla\boldsymbol{u}\big)\boldsymbol{n} &= \overline{\boldsymbol{t}} \quad \text{on} \quad \Gamma_{\boldsymbol{t}}\,, \end{aligned} \tag{8}$$

where the bar over the variable indicates that its values are known or prescribed and $\boldsymbol{n}$ denotes the unit outer vector normal to the boundary. The initial condition must be divergence free and will be denoted by $\boldsymbol{u}_0$.

2.2 Weak Form

Choosing arbitrary functions $\boldsymbol{w}$ and q from special subspaces for the velocities and pressure test functions, we can write the system of partial differential equations described by Eqs. (7) in an equivalent manner as

$$\big(\boldsymbol{w},\dot{\boldsymbol{u}}\big)_{\Omega} + \big(\boldsymbol{w},\big(\nabla\boldsymbol{u}\big)\boldsymbol{u}\big)_{\Omega} - \big(\boldsymbol{w},\nu\nabla^2\boldsymbol{u}\big)_{\Omega} + \big(\boldsymbol{w},\nabla p\big)_{\Omega} + \big(q,\mathrm{div}\boldsymbol{u}\big)_{\Omega} = \big(\boldsymbol{w},\boldsymbol{b}\big)_{\Omega}\,. \tag{9}$$

Now, integrating by parts the viscous and pressure terms, the previous equation results in

$$\begin{aligned} &\big(\boldsymbol{w},\dot{\boldsymbol{u}}\big)_{\Omega} + c\big(\boldsymbol{u};\boldsymbol{w},\boldsymbol{u}\big) + a\big(\boldsymbol{w},\boldsymbol{u}\big) - \big(p,\mathrm{div}\boldsymbol{w}\big)_{\Omega} + \big(q,\mathrm{div}\boldsymbol{u}\big)_{\Omega} \\ &+\big(p,\boldsymbol{w}\cdot\boldsymbol{n}\big)_{\Gamma} - \big(\nu\boldsymbol{w},(\nabla\boldsymbol{u})\boldsymbol{n}\big)_{\Gamma} = \big(\boldsymbol{w},\boldsymbol{b}\big)_{\Omega}\ . \end{aligned} \tag{10}$$

The integral on Γ vanishes at Γ_u because of the test function. The Neumann boundary conditions are applied as usual using the second expression of Eqs. (8). Thus the previous equation can be rewritten as

$$\begin{aligned} &\big(\boldsymbol{w},\dot{\boldsymbol{u}}\big)_{\Omega} + c\big(\boldsymbol{u};\boldsymbol{w},\boldsymbol{u}\big) + a\big(\boldsymbol{w},\boldsymbol{u}\big) - \big(p,\mathrm{div}\boldsymbol{w}\big)_{\Omega} + \big(q,\mathrm{div}\boldsymbol{u}\big)_{\Omega} \\ &-\big(\boldsymbol{w},\overline{\boldsymbol{t}}\big)_{\Gamma_t} = \big(\boldsymbol{w},\boldsymbol{b}\big)_{\Omega}\ , \end{aligned} \tag{11}$$

which is the weak form of the Navier-Stokes equation for incompressible fluid flow problems. The convective and viscous terms are written in the compact notation defined by the respective trilinear and bilinear forms

$$c\big(\boldsymbol{u};\boldsymbol{w},\boldsymbol{u}\big) = \int_{\Omega} \boldsymbol{w}\cdot(\nabla\boldsymbol{u})\boldsymbol{u}\,d\Omega \quad \text{and} \quad a\big(\boldsymbol{w},\boldsymbol{u}\big) = \int_{\Omega} \nabla\boldsymbol{w} : \nabla\boldsymbol{u}\,d\Omega\,.$$

2.3 Time Integration

The time integration scheme adopted here to solve the Navier-Stokes equations is the generalized midpoint rule (see [13]). In this method, the velocity is discretized in time as

$$\dot{\boldsymbol{u}}^{n+\gamma} = \frac{\boldsymbol{u}^{n+1} - \boldsymbol{u}^{n}}{\Delta t}\ , \quad \boldsymbol{u}^{n+\gamma} = \gamma\boldsymbol{u}^{n+1} + (1-\gamma)\boldsymbol{u}^{n}\ , \tag{12}$$

where $0 \le \gamma \le 1$. If γ is chosen to be equal to one, the backward Euler method is achieved. This is a very popular method and of easy implementation and, for simplicity, if we write the Navier-Stokes equation in (7) and its boundaries conditions in Eq.(8) using the backward

Euler time discretization scheme, we have

$$\begin{cases} \dfrac{\boldsymbol{u}^{n+1}-\boldsymbol{u}^{n}}{\Delta t}+\left(\nabla \boldsymbol{u}^{n+1}\right)\boldsymbol{u}^{n+1}-\nu\nabla^{2}\boldsymbol{u}^{n+1}+\nabla p^{n+1}=\boldsymbol{b}^{n+1} & \text{in } \Omega \\ \operatorname{div}\boldsymbol{u}^{n+1}=\boldsymbol{0} & \text{in } \Omega \\ \boldsymbol{u}^{n+1}=\overline{\boldsymbol{u}} & \text{on } \Gamma_{u} \\ -p^{n+1}\boldsymbol{n}+\nu\left(\nabla \boldsymbol{u}^{n+1}\right)\boldsymbol{n}=\overline{\boldsymbol{t}}^{n+1} & \text{on } \Gamma_{\boldsymbol{t}} \end{cases} \tag{13}$$

which is the semi-discrete system of equations for incompressible viscous fluid flow. The superscript 'n+1' is the time-step subsequent to 'n'.

2.4 Stabilization of the Finite Element Formulation

It is well known that incompressible fluid flow problems, when solved by the finite element method, have two sources of instabilities. The first arises from the Inf-Sup incompatibility condition and the second from convective dominated problems. There are several techniques to stabilize these problems and the one that was applied to this formulation is based on [8] for the Stokes problem. So we add the following stabilization terms to both the weak form of momentum conservation equation as well as to the incompressibility condition.

$$\begin{cases} a\left(\boldsymbol{w}^{h},\boldsymbol{u}^{h}\right)-\left(\operatorname{div}\boldsymbol{w}^{h},p^{h}\right)_{\Omega}+\sum_{e=1}^{nel}\tau_{e}\left(-\nu\nabla^{2}\boldsymbol{w}^{h},-\nu\nabla^{2}\boldsymbol{u}^{h}+\nabla p^{h}-\boldsymbol{b}^{h}\right)_{\Omega^{e}} \\ \qquad\qquad =\left(\boldsymbol{w}^{h},\boldsymbol{b}^{h}\right)_{\Omega}+\left(\boldsymbol{w}^{h},\overline{\boldsymbol{t}}^{h}\right)_{\Gamma_{t}} \\ \left(\operatorname{div}\boldsymbol{u}^{h},q^{h}\right)_{\Omega}-\sum_{e=1}^{nel}\tau_{e}\left(-\nabla q^{h},-\nu\nabla^{2}\boldsymbol{u}^{h}+\nabla p^{h}-\boldsymbol{b}^{h}\right)_{\Omega^{e}}=0\,, \end{cases} \tag{14}$$

where the indices 'h' means the discretized approximating or test functions. The value of τ_e depends on the kinematic viscosity and the element size. The stabilization of the transient Navier-Stokes problem is done based on the ideas by [9]. So the convection is stabilized by the addition of a SUPG term to the weak form as shown in Eq. (13).

$$\begin{cases} \left(\boldsymbol{w}^{h},\dot{\boldsymbol{u}}^{h}\right)_{\Omega}+c\left(\boldsymbol{u}^{h};\boldsymbol{w}^{h},\boldsymbol{u}^{h}\right)+a\left(\boldsymbol{w}^{h},\boldsymbol{u}^{h}\right)+\left(\operatorname{div}\boldsymbol{w}^{h},p^{h}\right)_{\Omega}-\left(\boldsymbol{w}^{h},\boldsymbol{b}^{h}\right)_{\Omega} \\ \qquad -\left(\boldsymbol{w}^{h},\overline{\boldsymbol{t}}^{h}\right)_{\Gamma_{t}}+\sum_{e=1}^{nel}\tau_{SUPG}\left((\nabla\boldsymbol{w}^{h})\boldsymbol{u}^{h},\mathcal{R}(\boldsymbol{u}^{h})\right)_{\Omega^{e}}=0 \\ \left(\operatorname{div}\boldsymbol{u}^{h},q^{h}\right)_{\Omega}=0\,. \end{cases} \tag{15}$$

Here, $\mathcal{R}(\boldsymbol{u}^h)$ is the residual of the momentum equation defined by

$$\mathcal{R}(\boldsymbol{u}^h) = \dot{\boldsymbol{u}}^h + \Big(\nabla \boldsymbol{u}^h\Big)\boldsymbol{u}^h - \nu\nabla^2\boldsymbol{u}^h + \nabla p^h - \boldsymbol{b}^h\,.$$

3 IMPOSING THE INTERFACE CONDITION BY XFEM

Our idea here is to use the XFEM approach described in [1] to simulate a moving interface between the fluid and structural domains. This technique allows the computation of the fluid flow variables from an Eulerian fixed grid in which the elements intersected by the structural wet surface are enriched in order to account for the velocity and pressure discontinuities. Note also that, in general, the structural wet surface does not match the fluid grid nodes, so the fluid velocities at the interface must be weakly enforced. For that purpose, we define a domain Ω that contains the fluid domain Ω_f and extends (for some portion) into the structural domain. So the interface Γ^i, see Figure 1, between the fluid and the structure will divide the fluid domain in two subdomains Ω^+ and Ω^- , the second having no physical meaning.

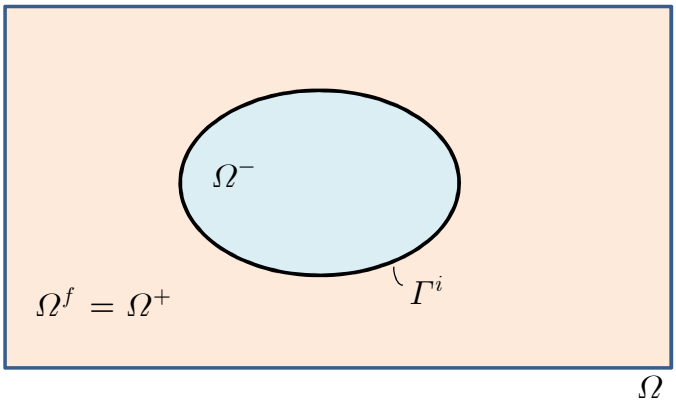

Figure 1. Decomposition of the fluid domain into Ω^+ and Ω^-.

The elements belonging to Ω^- are deactivated during computation and so memory and time processing is saved. Now, to ensure the fluid velocity compatibility at the interface, we must have

$$\boldsymbol{u} = \overline{\boldsymbol{u}}^i \quad \forall\, \boldsymbol{x} \in \Gamma^+ \tag{16}$$

and

$$-p\boldsymbol{n} + \nu(\nabla u)\boldsymbol{n} = 0 \quad \forall\, \boldsymbol{x} \in \Gamma^- \,. \tag{17}$$

Where the signal + or – at Γ refers from where we approximate to the interface, from Ω^+ or Ω^-, respectively. The interface condition between the fluid and the structure is weakly enforced by the product of the test function $\delta\boldsymbol{\lambda}$ of the Lagrange multiplier and the condition in Eq. (16) along Γ^+. This term must be added to Eq. (9) and the weak form needs to be recalculated. Thus, integrating by parts the viscous and pressure terms, a new term arises from the pseudo traction acting along the interface Γ^+:

$$\begin{aligned}&\big(\boldsymbol{w},\dot{\boldsymbol{u}}\big)_\Omega + c\big(\boldsymbol{u};\boldsymbol{w},\boldsymbol{u}\big) + a\big(\boldsymbol{w},\boldsymbol{u}\big) - \big(p,\mathrm{div}\boldsymbol{w}\big)_\Omega + \big(q,\mathrm{div}\boldsymbol{u}\big)_\Omega \\ &-\big(\boldsymbol{w},\overline{\boldsymbol{t}}\big)_{\Gamma_t} - \big(\boldsymbol{w},\boldsymbol{\lambda}\big)_{\Gamma^+} - \big(\delta\boldsymbol{\lambda},\boldsymbol{u}-\overline{\boldsymbol{u}}_i\big)_{\Gamma^+} = \big(\boldsymbol{w},\boldsymbol{b}\big)_\Omega\,.\end{aligned} \tag{18}$$

Here again the integral on Γ vanishes at Γ_u because of the test function. On Γ^+, the pseudo traction corresponds to the Lagrange multiplier.

3.1 Space Discretization by Finite Elements

This work adopts a mixed formulation in the sense that the finite elements have two unknowns (velocity and pressure) as primitive variables. Thus the approximating and test functions for the velocities and pressures can be written as

$$\begin{aligned} \boldsymbol{u}^h(\boldsymbol{x},t) &= \boldsymbol{N}_{\boldsymbol{u}}(\boldsymbol{x})\left(\boldsymbol{u}_e + H(\boldsymbol{x},t)\hat{\boldsymbol{u}}_e\right), \\ \boldsymbol{w}^h(\boldsymbol{x}) &= \boldsymbol{N}_{\boldsymbol{u}}(\boldsymbol{x})\left(\boldsymbol{w}_e + H(\boldsymbol{x},t)\hat{\boldsymbol{w}}_e\right), \\ p^h(\boldsymbol{x}) &= \boldsymbol{N}_p(\boldsymbol{x})\left(\boldsymbol{p}_e + H(\boldsymbol{x},t)\hat{\boldsymbol{p}}_e\right), \\ q^h(\boldsymbol{x}) &= \boldsymbol{N}_p(\boldsymbol{x})\left(\boldsymbol{q}_e + H(\boldsymbol{x},t)\hat{\boldsymbol{q}}_e\right). \end{aligned} \tag{19}$$

where $\boldsymbol{N}_{\boldsymbol{u}}$ and $\boldsymbol{N}_p$ are the matrixes of element shape functions for the velocity and pressure and $\boldsymbol{u}_e$ and $\boldsymbol{p}_e$ the vectors of element standard nodal velocities and pressure, respectively. $\hat{\boldsymbol{u}}_e$ and $\hat{\boldsymbol{p}}_e$ are the degrees of freedom belonging to the enhanced elements cut by Γ^i. These degrees of freedom must be multiplied by special enrichment functions $H(\boldsymbol{x},t)$ to account for velocities and pressure discontinuities across Γ^i. As the velocities and pressure must be zero in Ω, $H(\boldsymbol{x},t)$ can be defined by

$$H(\boldsymbol{x},t) = \begin{cases} 1 & \text{if } \boldsymbol{x} \in \Omega^+ \\ 0 & \text{if } \boldsymbol{x} \in \Omega^-. \end{cases} \tag{20}$$

To discretize the interface, linear functions were used for the Lagrange multiplier field as well as for its test function. Thus, we have

$$\boldsymbol{\lambda}^h = \boldsymbol{N}_\lambda(\boldsymbol{x},t)\lambda_e \quad \text{and} \quad \delta\boldsymbol{\lambda}^h = \boldsymbol{N}_\lambda(\boldsymbol{x},t)\delta\lambda_e. \tag{21}$$

As already stated in [1] and [10], the choice of the Lagrange multiplier subspace cannot be taken arbitrary because of instabilities purposes. Here we use linear approximating functions for the Lagrange multiplier subspace together with Q2Q1 Taylor-Hood element and no instabilities were observed on the examples performed.

3.2 Matrix Problem

Now if we substitute the approximating and test functions from (19) and (21) into the weak form (18) and discretize in time using the backward Euler method, after some algebraic manipulation it results in the following system of algebraic equations

$$\begin{bmatrix} \dfrac{\boldsymbol{M}}{\Delta t} + \boldsymbol{C} + \boldsymbol{K} & \boldsymbol{G} & -\boldsymbol{M}_\lambda^T \\ \boldsymbol{G}^T & \boldsymbol{0} & \boldsymbol{0} \\ -\boldsymbol{M}_\lambda & \boldsymbol{0} & \boldsymbol{0} \end{bmatrix} \begin{bmatrix} \boldsymbol{u}^{n+1} \\ \boldsymbol{p}^{n+1} \\ \boldsymbol{\lambda}^{n+1} \end{bmatrix} = \begin{bmatrix} \dfrac{\boldsymbol{M}}{\Delta t}\boldsymbol{u}^n + \boldsymbol{f}^{n+1} \\ \boldsymbol{0} \\ -\boldsymbol{M}_\lambda \overline{\boldsymbol{u}}_i \end{bmatrix}, \tag{22}$$

where $\boldsymbol{M}$, $\boldsymbol{C}$ and $\boldsymbol{K}$ are the usual mass, convective and viscous matrixes and $\boldsymbol{G}$ and $\boldsymbol{G}^T$ are the gradient and divergent operators, respectively. $\boldsymbol{M}_\lambda$ is defined by

$$\boldsymbol{M}_\lambda = \int_{\Gamma^+} \boldsymbol{N}_\lambda^T \boldsymbol{N}_u d\Gamma^+ \tag{23}$$

To solve the nonlinear system of equations in (22), the Newton-Raphson method was used.

4 COUPLED FSI PROBLEM

The algorithm used to solve the coupled fsi problem is based on a staggered scheme and is resumed below

Algorithm for the staggered scheme:

1) Estimate a trial position for the structural interface displacements $\boldsymbol{d}_{\Gamma,0}^{n+1}$ at the new time step n+1;
2) Fluid Problem: compute Dirichlet b.c. at interface and solve fluid field, including interface traction $\boldsymbol{t}_{\Gamma,i}^{f,n+1}$;
3) Structural Problem: use fluid traction at the interface computed from previous step and solve structural field. Obtain new position of the interface $\tilde{\boldsymbol{d}}_{\Gamma,i}^{n+1}$;
4) Relaxation of interface displacements: use Aitken relaxation parameter to predict the interface position for the next iteration $\boldsymbol{d}_{\Gamma,i}^{n+1} = \omega_i \tilde{\boldsymbol{d}}_{\Gamma,i}^{n+1} + (1-\omega_i)\tilde{\boldsymbol{d}}_{\Gamma,i-1}^{n+1}$;
5) Check convergence. If not satisfied, go back to step 2).

5 NUMERICAL RESULTS

This section presents some simulations carried in order to validate the formulation. The graphical interface was built with the help of the Gid Pre and Postprocessor software [14].

5.1 Steady flow around a cylinder

This example is a popular problem on incompressible viscous fluid flow simulation using the finite element method. Many references about this problem can easily be found in [9], [11], [12] and [13], for example. Here the inlet flow is uniform and the cylinder is placed at the centerline between two slip walls. The distances from the inlet wall and the slip walls to the center of the cylinder are 4.5D, where D is the diameter of the cylinder and takes the value of one. Total length of the domain is 20D. The inlet horizontal velocity was assumed to be unity and the vertical component was assumed zero all over top, bottom and left boundary. The right boundary was assumed to be open. The domain was discretized by 2000 Q2Q1 elements

and 8181 nodes, see Figure 2. The density and kinematic viscosity were defined as unity and 1/100, respectively, thus resulting in Re=100. The cylinder will be considered as a rigid body, thus no mesh was built for it.

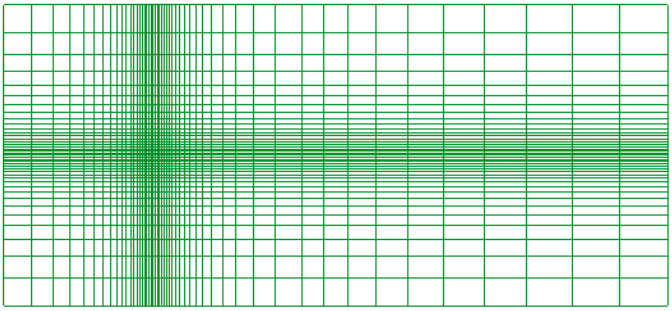

Figure 2. Mesh: 2000 Q2Q1 elements and 8181 nodes.

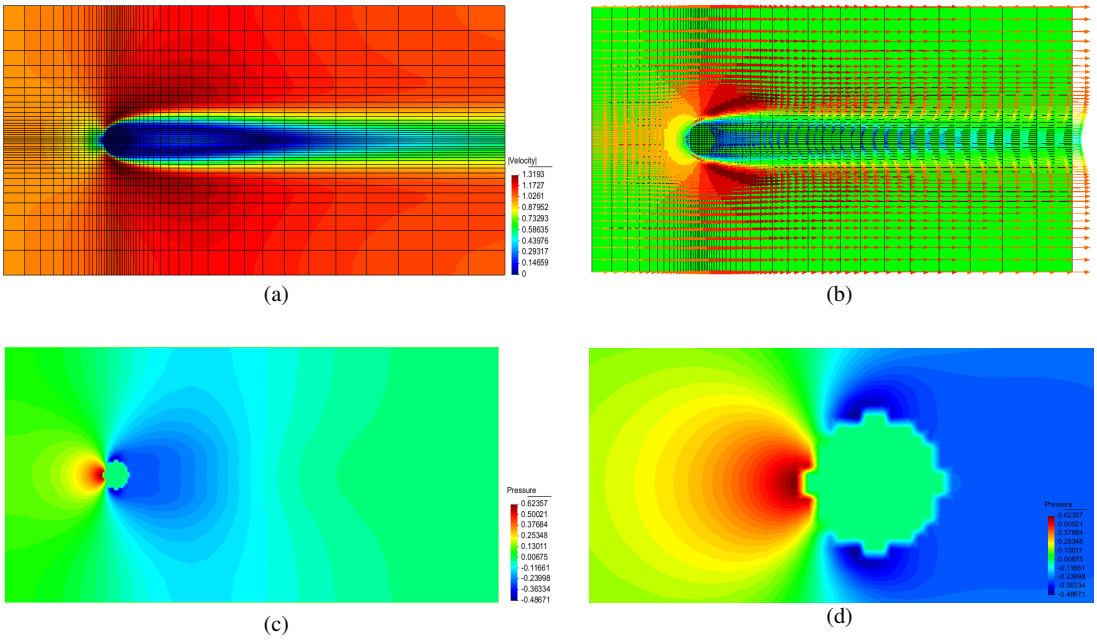

Figure 3. Velocity and pressure results for the steady flow past a cylinder and Re=100. (a) velocity contour fill; (b) velocity vectors; (c) pressure contour fill; (d) pressure contour fill detail.

Figure 3 shows the results for velocity and pressure. Notice in (d) that the pressure interpolation for post processing purpose was not done using the enrichment functions defined in Eq. (20). It is possible, however, to interpolate the pressure using the enhanced shape functions in order to calculate its values on Γ^+. Doing so, we could evaluate the pressure coefficient c_p around the cylinder surface and it is shown in Figure 4 (a). The Lagrange multipliers, in turn, are displayed in Figure 4 (b).

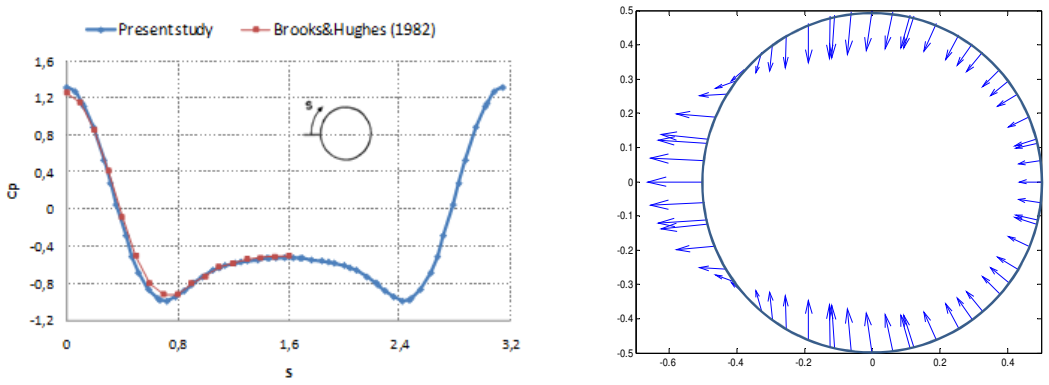

(a) (b)

Figure 4. (a) Pressure coefficient c_p and (b) Lagrange multipliers.

5.2 Unsteady flow around a moving cylinder

This example was performed in two steps. On the first step, the cylinder was kept fixed and the simulation was carried until the vortex shedding gets stable. The parameters are the same form previous example but a coarser mesh with 1200 elements and 4941 nodes was adopted. The time step used was 0.05s. At least two iterations were performed for each time step. Figure 5 shows the results for the velocities and pressure contour fill for two different instants of time. At 26s, a symmetric solution can still be observed and it is displayed in (a) and (b). After 94s of simulation, the vortex shedding is stable and the results are displayed in (c) and (d). On the second step, it was imposed a vertical movement to the cylinder at a low speed compared to 10% of the inlet horizontal velocity. So the cylinder center was forced to undergo an upward movement until a distance of 1.5D from its original position and after that it was forced to go down the same amount. As we are using a relative coarse mesh, the results of velocity contour fill in Figure 6 are displayed for qualitative purposes only. The results were taken from several instants of time so the whole movement of the cylinder can be caught by the reader. The offset distance at the legend means the distance from the cylinder center to its original position.

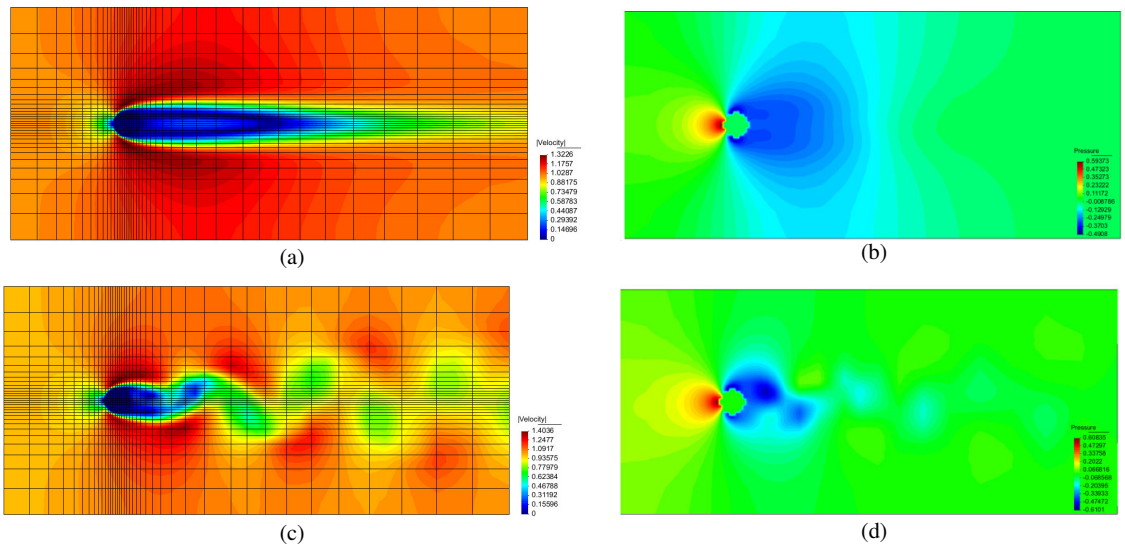

(a) (b)

(c) (d)

Figure 5. Velocity and pressure results for the unsteady flow past a cylinder and Re=100. (a) and (b) symmetric solutions for t=26s; (c) and (d) solutions after vortex shedding stabilization for t=94s.

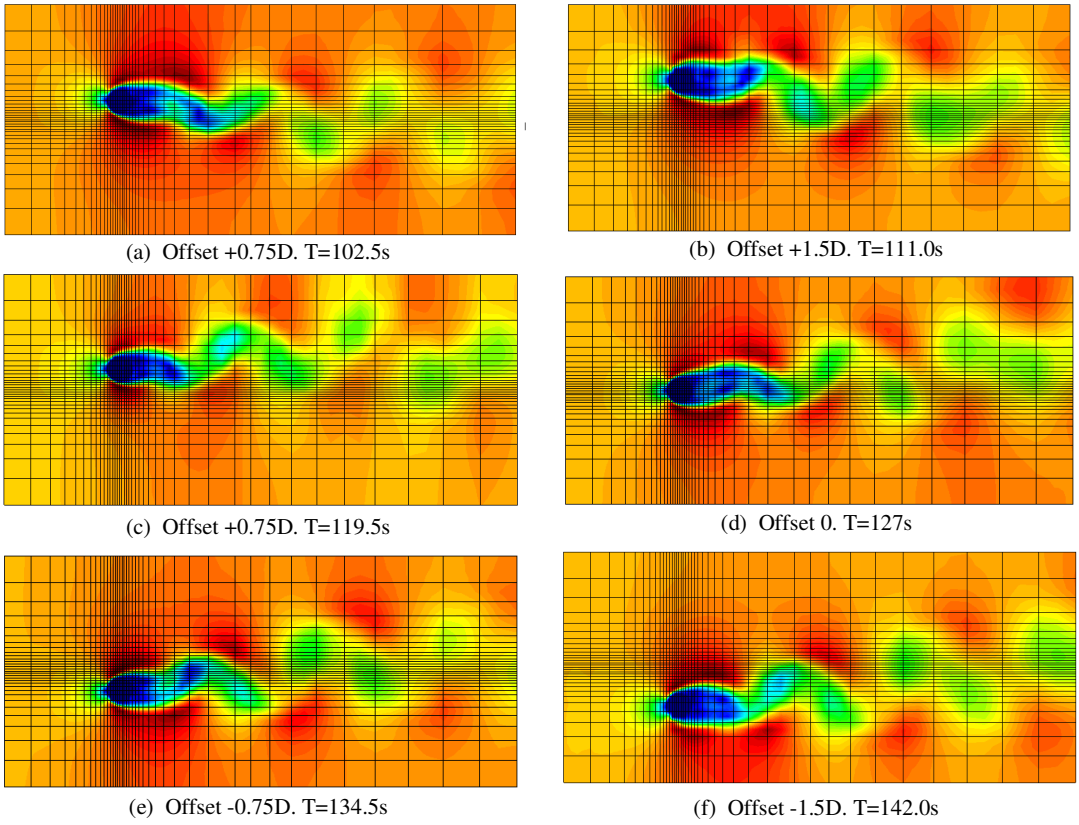

(a) Offset +0.75D. T=102.5s

(b) Offset +1.5D. T=111.0s

(c) Offset +0.75D. T=119.5s

(d) Offset 0. T=127s

(e) Offset -0.75D. T=134.5s

(f) Offset -1.5D. T=142.0s

Figure 6. Velocity contour fill for the moving cylinder.

5.3 Stationary flow through a channel with elastic structure

This example is very simple and consists of a stationary flow through a channel with an elastic structure as an obstacle. The top and the bottom of the channel have zero velocity prescribed while the outflow boundary is of zero traction type. Inflow horizontal velocity has a parabolic profile with unity value at the midheight. Inflow vertical velocity is zero. The fluid density and viscosity are equal to one and again the Taylor-Hood Q2Q1 element was adopted. The Kirchhof-St.Venant material in plane strain was used in the formulation of the structure problem with Young modulus E=5200 and Poisson coefficient equal to 0.48. In the discretization, 20 quadrilateral elements with 9 nodes were used. Figure 7 shows the the velocity and pressure contour fill for qualitative purposes.

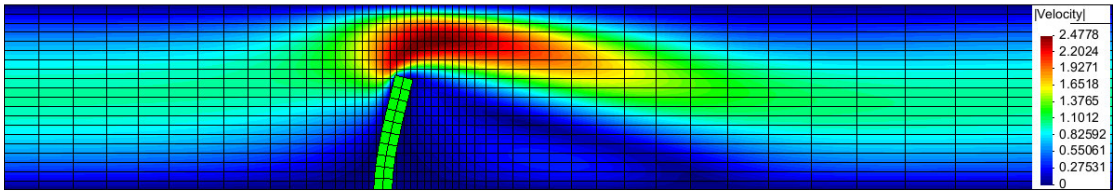

Figure 7. Velocity and pressure contour fill.

6 CONCLUSIONS

This work presented a study on XFEM to treat the interface between fluid and structural domains on FSI problems. It was shown that the Q2Q1 Taylor-Hood finite element can be safely combined with linear interpolated Lagrange multipliers on $\vec{\Gamma}$ and thus can be used for 2D FSI applications. The examples performed here had mostly qualitative purposes and more quantitative analyses are to be published in an upcoming paper. Even though the steady flow past the cylinder in section 5.1 shows very good agreement for the c_p distribution when compared to similar simulations as in [12].

ACKNOWLEDGEMENTS

This work was supported by the John Argyris Foundation, the CNPq (Conselho Nacional de Desenvolvimento Científico e Tecnológico) and by the DAAD (Deutscher Akademischer Austausch Dienst).

REFERENCES

[1] A. Gerstenberger, W.A. Wall, An eXtended Finite Element Method/Lagrange multiplier based approach for fluid-structure interaction, Comput. Methods Appl. Mech. Engrg. v. 197 p. 1699-1714, 2008.

[2] S.R. Idelson et al., Unified Lagrangian formulation for elastic solids and incompressible fluids: Application to fluid-structure interaction problems via the PFEM, Comput. Methods Appl. Mech. Engrg. (2007).

[3] E. Oñate et al., Advances in the particle finite element method for the analysis of fluid-structure interaction and bed erosion in free surface flows, Comput. Methods Appl. Mech. Engrg. (2007).

[4] H.C. Gomes, P.M. Pimenta. Mixed Triangular Finite Element Applied to Incompressible Fluid Flow Problems, Presented in: XXX Iberian Latin-American Congress on Computational Methods in Engineering - CILAMCE. Búzios, RJ, November 08 to 11, 2009. ABMEC, COPPE/UFRJ and LNCC.

[5] Küttler, U., Wall, W.A. Fixed-point fluid–structure interaction solvers with dynamic relaxation. Computational Mechanics.43 (2008) 61-72.

[6] Temam, R. Navier-Stokes equations: theory and numerical analysis. North-Holland, Amsterdam, 1984.

[7] J. Donea, A. Huerta, The Finite Element Method for Flow Problems, John Wiley, 2003.

[8] Hughes, T.J.R. and Franca, L.P.(1987), A new finite element formulation for computational fluid dynamics. VII. The Stokes problem with various well-posed boundary conditions: symetric formulations that converge for all velocity/pressure spaces, Comput. Methods Appl. Mech. Eng. 65(1), 85-96.

[9] Tezduyar, T.E. Osawa, Yasuo. Finite Element Stabilization Parameters Computed from Element Matrices and Vecors, Comput. Methods Appl. Mech. Engrg.190 (2000) 411-430.

[10] N. Möes, E. Béchet, M. Tourbier, Imposing Dirichlet boundary conditions in the extended finite element method, Int. J. Numer. Methods Engrg. 67 (12) (2006) 1641-1669.

[11] Zienkiewicz O. C. and Taylor R. L., The Finite Element. Method. Fluid Dynamics. Vol. 3, McGraw-Hill, London, 2000.

[12] Brooks, T.J.R. Hughes, Streamline upwind/Petrov-Galerkin formulation for convection dominated flows with particular emphasis on the incompressible Navier-Stokes equations, Comput. Methods Appl. Mech. Eng. 32 (1982) 199-259.

[13] W. Dettmer, D. Perić, An analyses of the time integration algorithms for the finite element solutions of incompressible Navier-Stokes equations based on a stabilized formulation, Comput. Methods Appl. Mech. Engrg. 192 (2003) 1177-1226.

[14] Gid, The Personal Pre and PostProcessor. Version 9.0.2, International Center for Numerical Methods in Engineering CIMNE, 2008.